Electronic Supplementary Material (ESI) for Catalysis Science & Technology.
This journal is © The Royal Society of Chemistry 2020

Selective formic acid dehydrogenation at low temperature over RuO_2/COF pre-catalyst synthesized on the gram scale

Liliana P. L. Gonçalves,[a, b] David B. Christensen,[c] Maria Meledina,[d,e] Laura M. Salonen,[a] Dmitri Y. Petrovykh,[a] Juliana P. S. Sousa,[a] O. Salomé G. P. Soares,[b] Enrique Carbó-Argibay,[a] M. Fernando R. Pereira,[b] Søren Kegnæs,[c,*] Yury V. Kolen'ko,[a,*]

[a] *International Iberian Nanotechnology Laboratory (INL), Avenida Mestre José Veiga, 4715-330 Braga, Portugal*
**e-mail:* yury.kolenko@inl.int (Yu. V. Kolen'ko)
[b] *Laboratory of Separation and Reaction Engineering – Laboratory of Catalysis and Materials (LSRE-LCM), Faculdade de Engenharia, Universidade do Porto, Rua Dr. Roberto Frias, 4200-465 Porto, Portugal*
[c] *Technical University of Denmark, DTU Chemistry, Kemitorvet 207, 2800 Kgs. Lyngby, Denmark*
**e-mail:* skk@kemi.dtu.dk (S. Kegnæs)
[d] *RWTH Aachen University, Central Facility for Electron Microscopy, D-52074 Aachen, Germany*
[e] *Forschungszentrum Jülich GmbH, Ernst Ruska-Centre (ER-C 2), D-52425 Jülich, Germany*

* Corresponding authors
E-mail: yury.kolenko@inl.int (Yu. V. Kolen'ko); skk@kemi.dtu.dk (S. Kegnæs)

CHEMICALS

Hexamethylenetetramine, *o*-tolidine, and anhydrous phloroglucinol were purchased from TCI Chemicals, and $RuCl_x{\cdot}xH_2O$ was purchased from Alfa Aesar. All other reagents and solvents were purchased from Sigma-Aldrich and Fisher Scientific. Commercial reagents and solvents were used as received. Ultrapure water was produced by Milli-Q Advantage A10 system (Millipore; resistivity = 18.2 MΩ cm^{-1}). Reduced 5%Ru on activated carbon control catalyst was purchased from Alfa Aesar (11748). The S_{BET} of the catalyst is 720 m^2/g.

SYNTHESIS

Triformylphloroglucinol (Tp), was synthesized as follows:[22] hexamethylenetetraamine (15.10 g, 108 mmol) and phloroglucinol (6.01 g, 49 mmol) were placed in a three-necked round-bottom flask under N_2 and 90 mL of trifluoroacetic acid was added. The solution was heated to 100 °C for 2.5 h under inert atmosphere. Approximately 150 mL of aq. 3 M HCl was added and the solution was heated to 100 °C for 1 h. After cooling to room temperature, the solution was filtered and extracted with dichloromethane, dried over anhydrous sodium sulfate, filtered, and dried in a rotary evaporator.

For the synthesis of TpBD-Me_2 **COF**,[20] Tp (1.50 g, 7.14 mmol) and *o*-tolidine (1.52 g, 7.14 mmol) were placed in a pressure tube (ACE glass, bushing type back seal, 100 mL) under N_2 and then 60 mL of anhydrous 1,4-dioxane were added. The mixture was sonicated to obtain a homogeneous dispersion. Then, aq. 6 M acetic acid (4.16 mL, 25.0 mmol) was added to the mixture. The tube was flushed with N_2, closed, and heated in an oil bath to 120 °C for 3 days. The precipitate was collected by centrifugation (4400 rpm, 15 min), washed with acetone four times and collected by centrifugation (4400 rpm, 15 min), and washed with tetrahydrofuran by stirring the COF dispersed in the solvent and filtering under vacuum until the washing solvent was colorless. Finally, the material was dried at 120 °C under vacuum for 2 h to yield TpBD-Me_2 COF as ≈2 g of orange powder.

The **Ru-COF** pre-catalyst was prepared by precipitation of RuO_2 nanoparticles on TpBD-Me_2 COF support as follows:[23] the support (1.22 g) was suspended in aq. $RuCl_x \cdot xH_2O$ solution (71.5 mL, 0.6 mmol Ru, 8.3 mM). The mixture was left stirring at room temperature for 15 min in order to impregnate the precursor on the support. Then, aq. 1 M NaOH solution (14 mL) was added and the stirring continued for 18 h. Finally, the sample was filtered, washed with water until the filtrates were colorless, and dried under vacuum at 120 °C.

CHARACTERIZATION METHODS

N_2 Physisorption

The N_2 adsorption–desorption isotherms at –196 °C were recorded using a Quantachrome Autosorb IQ2 multi-station apparatus. Approximately 100 mg of sample was placed in the sample holder tube. The sample was degassed at 120 °C for 180 min. After that, the sample holder tube was placed into liquid nitrogen bath and the analysis was started. The specific surface area of the materials was determined by the BET method, and the total pore volume is calculated using the amount of vapor adsorbed at relative pressure close to unity ($P/P_0 = 0.97$) by assuming that the pores were filled with liquid adsorbate, and thus, converting the adsorbed volume in volume of liquid nitrogen. The pore size distribution was estimated using quenched solid density functional theory (QSDFT) approach for slit/cylindrical pores while treating the adsorption branch of the isotherm.

Small-Angle X-ray Scattering (SAXS)

The crystallinity of the material was evaluated by SAXS performed on an Anton Paar SAXSess mc^2 instrument operating at 40 kV and 50 mA. The samples were placed in a holder with Mylar windows for the measurement and the data was collected with an image plate detector. All data are background corrected.

Inductively Coupled Plasma–Optical Emission Spectroscopy (ICP–OES)

The ruthenium content was determined by ICP–OES using an ICPE-9000 Multitype ICP Emission Spectrometer from Shimadzu, equipped with a nebulizing system and using optical emission spectroscopy for detection. Samples were digested by dispersing 20 mg in 12 g of concentrated HNO_3 (65%) in an autoclave, which was kept in the oven at 180 °C for 12 h to completely decompose the sample. Subsequently, the acidic solution was diluted in a 50 mL volumetric flask and subjected to the chemical analysis. Measurements were repeated three times and the results are the mean value with relative standard deviation.

X-ray Photoelectron Spectroscopy (XPS)

XPS measurements were performed using a monochromated microfocused Al K_α X-ray source that defined an analysis spot of ca. 650 × 400 μm^2. The binding energy (BE) scale of the analyzer had been calibrated based on Au $4f_{7/2}$ reference BE value of 83.95 eV. All spectra were acquired in normal emission with an enabled magnetic lens, producing an effective analyzer collection angle of ca. 30°. Powdered samples were pressed into carbon tape, which was directly attached to the sample holder.

Charge neutralization was provided by beams of low-energy (≤10 eV) Ar^+ ions and electrons guided by the magnetic lens. For the complex powder of nanoporous COF, charge neutralization was challenging. Nevertheless, the standard acquisition conditions produced a local maximum in the neutralizer efficiency. For metallic Ru signal, the measured BEs were within 0.1–0.3 eV from the published reference values:[29] Ru $3d_{5/2}$ at 280.0 (Figure S3c) vs 279.9 eV and Ru $3p_{3/2}$ at 461.5 (Figure 1b) vs 461.2 eV, respectively. Accordingly, the BE values are reported as measured and assumed to be within <0.3 eV from values that could be obtained under perfect charge neutralization.

A convolution of Lorentzian and Gaussian lineshapes on a linear combination of Shirley and linear backgrounds was used to fit the individual components, choosing the minimal number of self-consistent components that were able to fit spectra across all the samples. The number of components for C 1s, N 1s, and O 1s spectra was fixed based on the fits for pristine COF sample (Figure S3a); the positions of C 1s components were constrained to small variations from their positions in the COF sample, when necessary for disambiguation of the fits for Ru 3d peaks.

The reported elemental ratios were estimated from the standard “atomic %” elemental compositions that were quantified using calibrated analyzer transmission functions, Scofield sensitivity factors, and TPP-2M effective attenuation lengths for photoelectrons, as implemented in Avantage software (Thermo Scientific).

Annular dark-field scanning transmission electron microscopy (ADF–STEM)

ADF–STEM and energy dispersive X-Ray spectroscopy in STEM mode (STEM–EDX) experiments were carried out using two FEI Titan transmission electron microscopes operated at an accelerating voltages of 200 kV (in the case of STEM–EDX mapping)[25,26] and 300 kV (in the case of high resolution imaging),[27] and both equipped with a probe spherical aberration corrector unit and one equipped with a Super-X EDX system. The samples were prepared by dispersing powder samples in ethanol and dropping the dispersion onto a carbon coated copper grid. The average particle size was determined before and after the catalytic testing by measuring at least 50 nanoparticles.

Catalytic Experiments

In order to test the performance of **Ru-COF** for formic acid dehydrogenation, 50 $cm^3\ min^{-1}$ of N_2 saturated with formic acid (roughly 10% FA) was passed over 10 mg of the catalyst. The catalyst was mixed with 90 mg of quartz (350–700 μm) to prevent the sample from clogging the system and the sample was heated and cooled at 1 °C min^{-1} in two cycles from 100 °C to 200 °C. CO_2 and CO content was measured using a Rosemount BINOS 100 detector.

Control 5 wt% Ru on activated carbon catalyst (**Ru-C**) was also tested under the same conditions as a comparison for our catalyst. To compensate for the difference in Ru loading, only 6 mg of the commercial **Ru-C** was used for the cycle experiments and 18 mg for the stability and plateau experiments, thereby keeping the amount of Ru equivalent.

Additionally, stability tests were performed under the same conditions, with the difference that, in this case, 30 mg of **Ru-COF** were used in order to obtain a reasonable yield. Note that due to the relatively low flow, few minutes are needed for the measured gas stream to reflect the change in the system when increasing the temperature.

The choice of temperature for the stability tests was made based on another set of experiments, in which the activity of the samples was determined at 120, 140, 160, 180, and 200 °C (Figure S7c). Results indicated that significant deactivation occurred at higher temperatures, and therefore the stability tests were carried out at 120 °C.

Conversion of formic acid (X), yield to hydrogen (Y_{H2}), and selectivity to hydrogen ( ) were calculated as follows, considering that the amount of H_2 formed corresponds to the amount of CO_2 formed ($HCOOH \rightarrow H_2 + CO_2$):

$$S_{H_2} = \frac{[CO_2]_{out}}{[CO_2]_{out} + [CO]_{out}} \times 100 \qquad \text{(S1)}$$

$$Y_{H_2} = \frac{[CO_2]_{out}}{[HCOOH]_{in}} \times 100 \qquad \text{(S2)}$$

$$X = \frac{Y_{H_2}}{S_{H_2}} \times 100 \qquad \text{(S3)}$$

The dispersion of the sample was calculated to be ≈100%, as follows:[35]

$$D(\%) = 6\,\frac{(v_m/a_m)}{d_p} \qquad \text{(S4)}$$

Where, D is the dispersion, d_p is the mean particle size, v_m is the volume occupied by an atom in bulk metal and a_m is the surface area occupied by an atom of metal on a polycrystalline surface.

CHARACTERIZATION RESULTS

COF structure

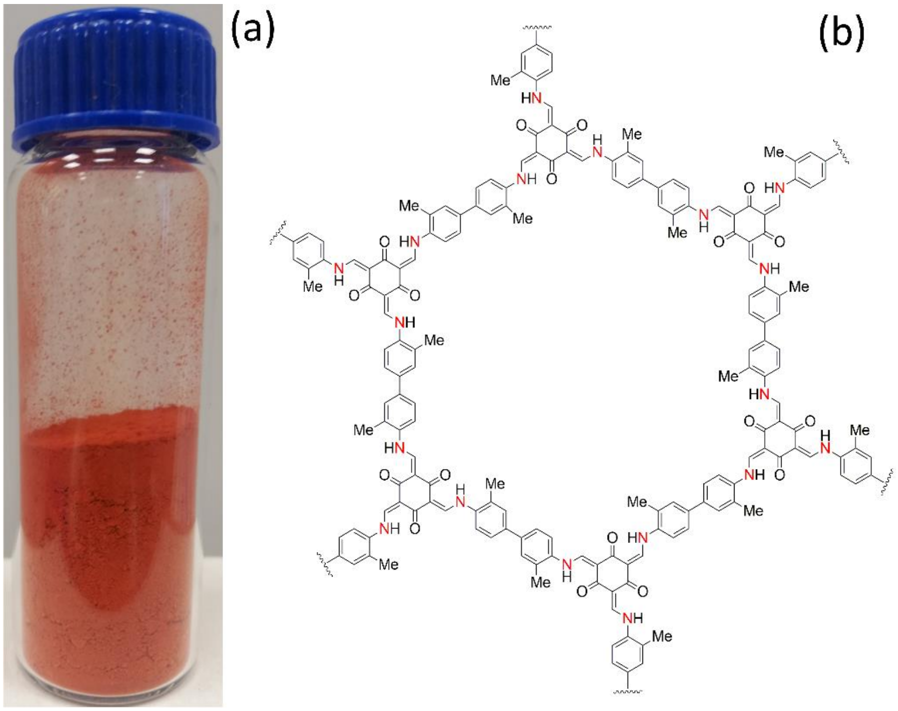

Figure S1. Photograph (a) and the chemical structure (b) of the synthesized ca. 2 g of TpBD-Me_2 **COF** powder.

N_2 physisorption

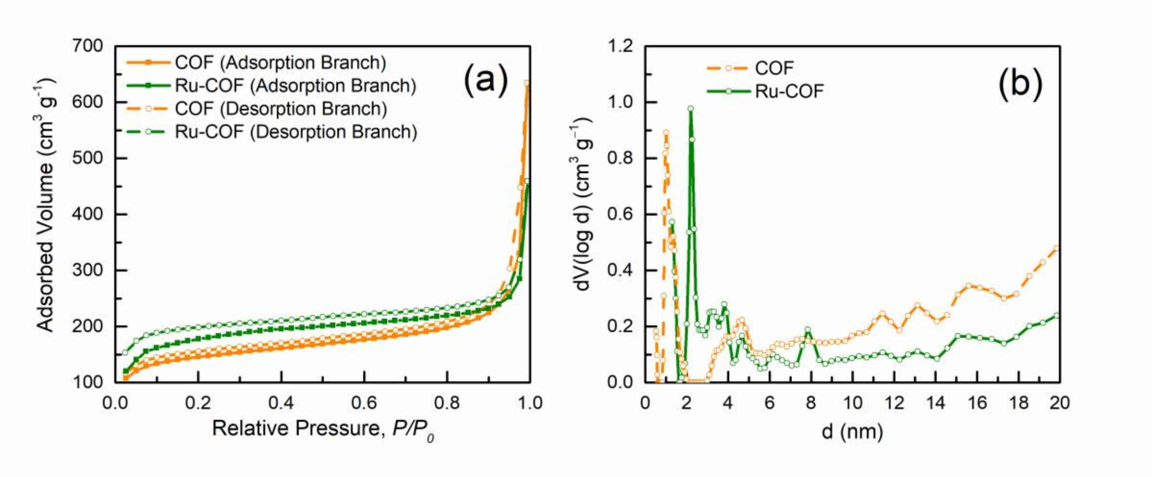

Figure S2. (a) N_2 adsorption–desorption isotherms and (b) pore size distribution of **COF** and **Ru-COF**.

Table S1. Textural properties of **COF** and **Ru-COF.**

Sample	***S_{BET}*** ***($m^2\ g^{-1}$)***	***d_p*** ***(nm)***	***V_p*** ***($cm^3\ g^{-1}$)***	***V_{micro}*** ***($cm^3\ g^{-1}$)***
COF	520	1.0	0.51	0.15
Ru-COF	630	1.3	0.44	0.23

X-ray photoelectron spectroscopy

The method for the RuO_2 NPs precipitation used in this work has been extensively reported in the literature and it has been proposed that the precipitated NPs are distinct in structure and composition from anhydrous RuO_2 and have been designated as "hydrated RuO_2" or "Ru hydroxide".[23] After extensive XPS analysis (Figure 1b), we conclude that our as-synthesized catalyst is predominantly composed of hydrated RuO_2.

Based on BEs of Ru in the XPS data, it is not possible to distinguish the hydrated and anhydrous forms of RuO_2, as has been demonstrated previously using different combinations of reference samples.[29-31] Techniques complementary to XPS have revealed that hydrated RuO_2 includes Ru with hydroxyl ligands,[28,30] however, stoichiometric $Ru(OH)_3$ would have the Ru $3p_{3/2}$ peak at BE ca. 1.5 eV higher than that in Figure 1b. The combination of literature results and our XPS data (Figure 1b and S3) thus indicates that Ru particles in the as-synthesized pre-catalyst are predominantly composed of hydrated RuO_2, which is characterized by the Ru chemical environment similar to, yet distinct from, Ru hydroxide.

The details of the spectra in C 1s (Ru 3d), N 1s, and O 1s regions in Figure S3 provide information about the chemistry of both the **COF** support and **Ru-COF**. The significant overlap between the peaks associated with **COF** and **Ru-COF** in both C 1s (Ru 3d) and O 1s regions highlights the importance of developing a self-consistent fitting model for the spectra of the "witness" **COF** sample, which has been treated with NaOH, to simulate preparing the **Ru-COF** but in absence of the catalyst precursors. The fitting model for this **COF** support (Figure S3a) is then used as the baseline for the interpretation of the spectra of the supported **Ru-COF** samples (Figure S3b and c).

Fitting the C 1s spectrum of the **COF** support in Figure S3a requires a minimum of three components and a π–π^* shakeup feature. While, in principle, adding one or two more components to the fit does improve the randomness of the fit residuals, it is difficult to maintain consistent fits across all three materials with so many components, without artificially restricting them. The minimal fit shown in Figure S3a, in contrast, is partially constrained by features in the raw data and results in a typical FWHM for each of the components for organic systems.[32] In agreement with the literature,[32] the three components correspond to (aromatic) C–C (BE = 283.9 ± 0.1 eV, FWHM = 1.4 ± 0.1 eV), a combination of C–N, C–O, C–CO (BE = 285.0 ± 0.1 eV), and C=O (BE = 287.2 ± 0.2 eV); the last two components are constrained to have identical FWHM, which in all the fits expanded to the upper limit of 1.9 eV. Without extensive additional characterization by complementary methods, the fit of the π–π^* shakeup feature is necessarily indicative and unstructured, with a single broad component at BE of 289.4–289.9 eV, consistent with the typical values for aromatic shakeup features.[32]

The spectra in the N 1s region in Figure S3 are particularly important as signatures of COF-specific molecular chemistry. In all cases, the spectrum includes the single primary peak at BE = 399.2 ± 0.1 eV (FWHM = 1.5 ± 0.1 eV) and two broad low-intensity shakeup features at 403.1 ± 0.3 eV and 406.0 ± 0.5 eV.

The minimal changes in the aromatic C–C and the imine N 1s peaks across all three samples provide evidence that no major chemical degradation (e.g., ring opening, oxidation, bond cleavage) of **COF** occurs during the synthesis of the **Ru-COF** or during the catalytic testing. The shakeup features in both C 1s and N 1s regions are even more sensitive to the molecular structure of the **COF** at the level of its unit cell and beyond, because resonant shakeup features require the presence of uniform and spatially ordered HOMO and LUMO energy bands. The clear presence of the shakeup features after the catalytic testing, therefore, provides strong evidence that the lateral chemical structure and ordering of the **COF** does not suffer significant degradation in the process.

Inferences about the chemistry of the **Ru-COF** from the spectra in Figure S3 are complementary to those discussed in the main text and Figure 1b. As-synthesized pre-catalyst produces the primary Ru $3d_{5/2}$ peak at 281.0 eV (Figure S3b), which is in excellent agreement with the value of 280.8 eV reported for hydrated RuO_2.[29] The additional Ru $3d_{5/2}$ component at 282.0 eV (Figure S3b) is just below the value of 282.3 eV reported for $Ru(OH)_3$,[29] in agreement with the expected presence of some OH ligands in the hydrated RuO_2.[28] The interpretation of complementary evidence from the O 1s region is only semi-quantitative, because the O 1s lineshape measured for the **COF** support (Figure S3a) is nearly identical, for example, to that reported for electrochemically grown hydrated RuO_2.[34] This unusual spectral overlap is partly the result of the intrinsic oxygen signal from C=O groups in the **COF** (confirmed by ca. 1:1 ratio to the C=O component in C 1s region) being at an unusually low (for oxygen in organic molecules) BE of 530.1 ± 0.1 eV, i.e., overlapping with the typical metal-oxide BE range. Nevertheless, the standard protocol for generating hydrated RuO_2 from $RuCl_3$ is expected to produce O 1s components at 530.4 and 532.7 eV,[28] which is reflected in the corresponding increase of O 1s components at 530.1 and 532.8 eV in the fits between Figure S3a and b. After the catalytic testing, the Ru $3d_{5/2}$ components shift to 280.0 and 281.5 eV (Figure S3c), the lower-BE one being in perfect agreement with BE = 279.9 eV expected for metallic Ru [28] and the higher-BE one corresponding to the remnants of the original hydrated RuO_2. Observing relatively stronger signals from the minority components in Ru 3d vs 3p region (the latter has a shallower sampling depth) also suggests that the corresponding chemical states of Ru are nonuniformly distributed, e.g., between the core and surface regions of the Ru catalyst particles.

XPS analysis of the sample after the catalytic testing (Figure1b and S3c) indicates that the chemical structure of the **COF** support remains largely unchanged. This is evidenced by the minimal changes in the resonant shakeup[32] features in the C 1s, N 1s, and O 1s spectra (Figure S3), which are produced by the combination of HOMO and LUMO bands specific to the molecular structure of the **COF**.

Based on the SAXS (Figure 1a) and XPS (Figure 1b and Figure S3) data, we believe that the loss of crystallinity is due to delamination of the **COF** into sheets, rather than a modification of its chemical structure. This phenomenon has been previously observed with COF catalysts, and has been attributed to weak interlayer interactions within the materials.[33] The presence of strong in-plane bonds and weaker van der Waals interactions between the layers in 2D COFs leads to the possibility of chemical or mechanical delamination and random displacement of 1D COF layers, which is reflected in the reduction of intensity of the main reflection observed in the SAXS pattern.[24]

After the catalytic testing the initial RuO_2 NPs undergo a dramatic transformation: the Ru $3d_{5/2}$ components shift to 280.0 and 281.5 eV (Figure S3c), the lower-BE one being in perfect agreement with BE = 279.9 eV expected for metallic Ru[29,34] and the higher-BE one corresponding to the remnants of the original hydrated RuO_2. Observing relatively stronger signals from the minority components in Ru 3d vs 3p region (the latter has a shallower sampling depth) also suggests that the corresponding chemical states of Ru are non-uniformly distributed, e.g., between the core and surface regions of the Ru catalyst particles. Some of the hydrated RuO_2, perhaps in the core of the particles, is not reduced during the catalytic testing.

Table S2 presents the elemental composition determined by XPS for **COF**, **Ru-COF**, and **Ru-COF** after catalytic testing. We note that for comparison with literature in the main text, the 8.9 atomic % of N in the **COF** was converted to 9.9 weight %, which is approximately correct because the atomic weights of C, N, an O (present in the **COF** support) are similar.

Table S2. Elemental composition determined by XPS for **COF**, **Ru-COF**, and **Ru-COF** after catalytic testing.

	C (at%)	*O (at%)*	*N (at%)*	*Ru (at%)*
COF	**81.0**	**10.1**	**8.9**	**0.0**
Ru-COF	**72.3**	**17.1**	**7.2**	**3.4**
Ru-COF after catalytic testing	**72.2**	**16.8**	**7.5**	**3.5**

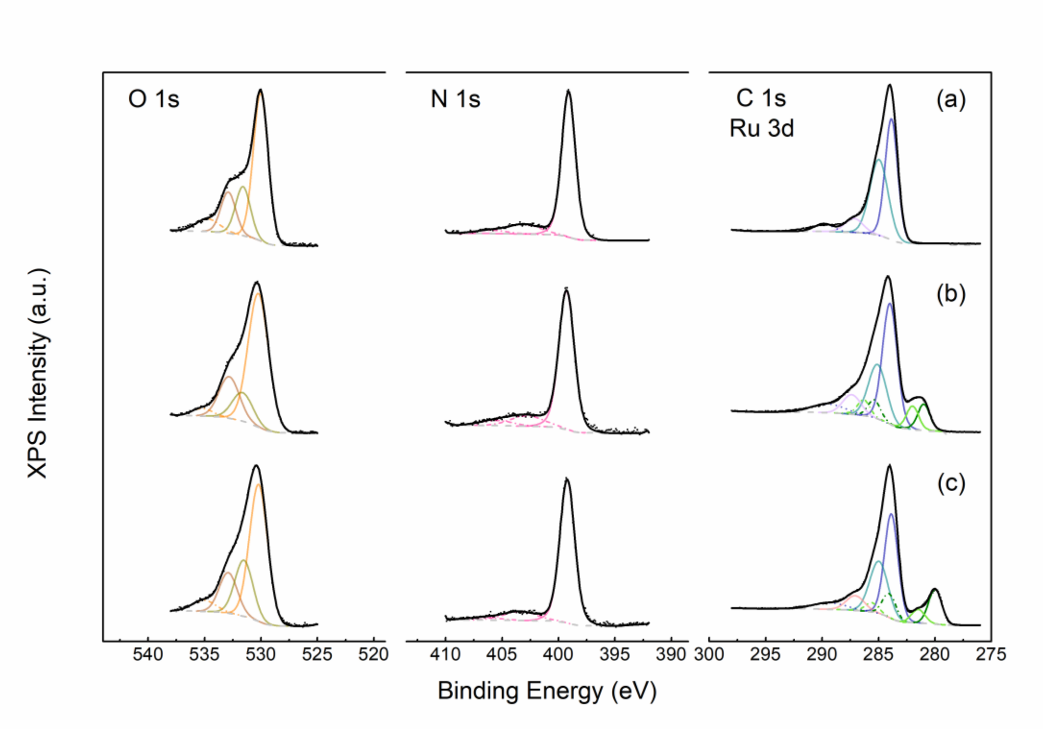

Figure S3. High-resolution XPS data for O 1s, N 1s and C1s/Ru 3d regions of (a) **COF** treated with NaOH, (b) **Ru-COF**, and (c) **Ru-COF** after stability test. Symbols: raw data; black lines: overall fits; colored lines: fits of individual components; grey dashed lines: background.

Electron microscopy

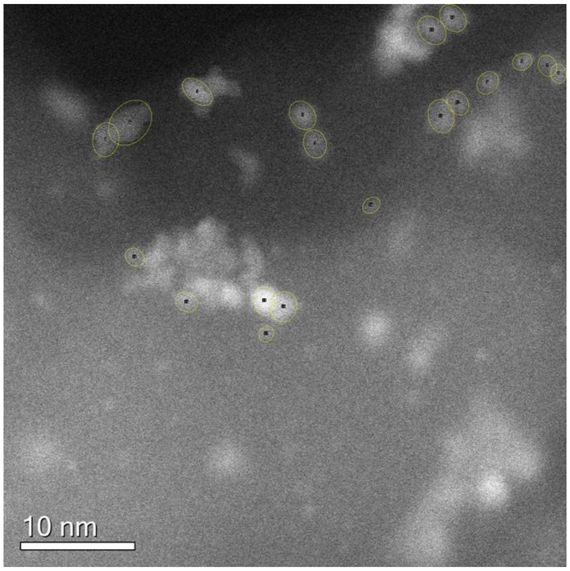

Figure S4. ADF–STEM image of **Ru-COF** showing the agglomerates found in the sample, composed by nanoparticles with ≈1.2 nm in diameter.

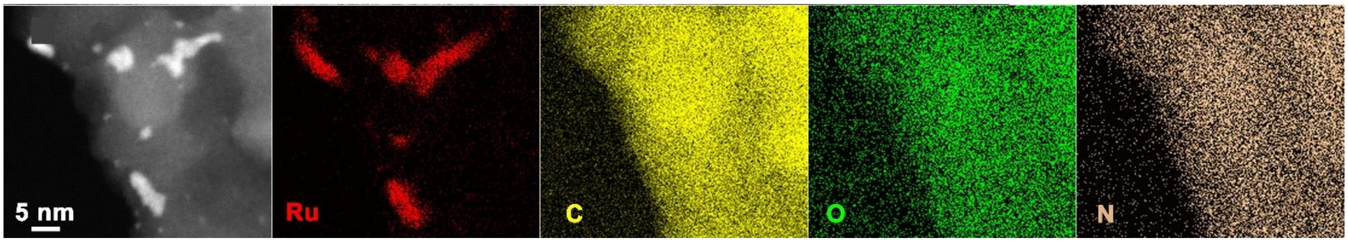

Figure S5. ADF–STEM image of **Ru-COF** with simultaneously collected EDX maps of Ru, C, O, and N.

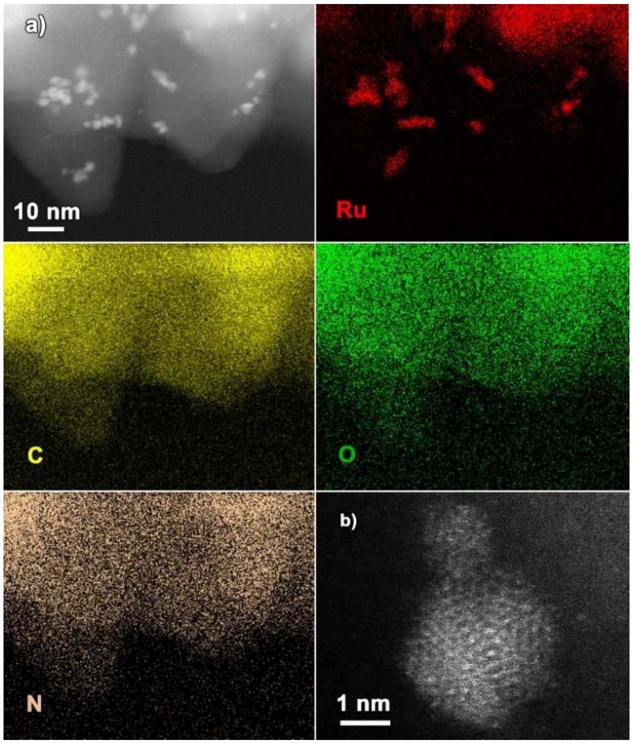

Figure S6. Morphology and chemical composition of **Ru-COF** after the catalytic test: (a) ADF–STEM overview together with the corresponding EDX maps for Ru, C, O, and N. (b) ADF–STEM image of a Ru nanoparticle.

The morphology and chemical composition of the material after the catalytic stability test (Figure S6) were analysed and the distribution of C, O, and N in the COF support remains homogeneous and the Ru NPs are decorating the **COF** support. Furthermore, we note that after catalysis the diameter of the Ru NPs increases up to ≈2.4 nm (Figure S6).

CATALYTIC EXPERIMENTS

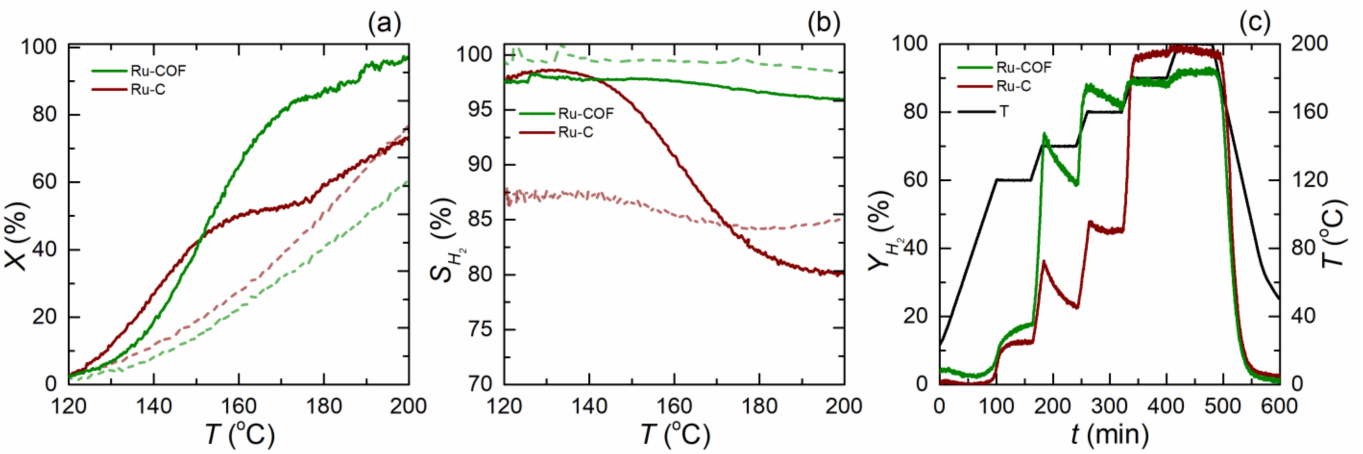

Figure S7. Comparison of catalytic performance of our catalyst and a commercial **Ru-C** catalyst in the dehydrogenation of formic acid. (a) Light-off curve for the conversion of formic acid (*X*) as a function of reaction temperature, (b) light-off curve for the selectivity to H_2 (S_{H2}) as a function of reaction temperature and (c) H_2 yield (Y_{H2}) as a function of time for different temperature steps (120, 140, 160, 180, and 200 °C). Green line: **Ru-COF**; brown line: **Ru-C**; solid line: first cycle; dashed line: second cycle; black line: temperature.